

# UC Irvine

## UC Irvine Previously Published Works

### Title

Space-based formaldehyde measurements as constraints on volatile organic compound emissions in east and south Asia and implications for ozone

### Permalink

<https://escholarship.org/uc/item/2239v12r>

### Journal

Journal of Geophysical Research, 112(D6)

### ISSN

0148-0227

### Authors

Fu, Tzung-May  
Jacob, Daniel J  
Palmer, Paul I  
[et al.](#)

### Publication Date

2007

### DOI

10.1029/2006jd007853

### Copyright Information

This work is made available under the terms of a Creative Commons Attribution License, available at <https://creativecommons.org/licenses/by/4.0/>

Peer reviewed

## Space-based formaldehyde measurements as constraints on volatile organic compound emissions in east and south Asia and implications for ozone

Tzung-May Fu,<sup>1</sup> Daniel J. Jacob,<sup>1</sup> Paul I. Palmer,<sup>2,3</sup> Kelly Chance,<sup>4</sup> Yuxuan X. Wang,<sup>1</sup> Barbara Barletta,<sup>5</sup> Donald R. Blake,<sup>5</sup> Jenny C. Stanton,<sup>6</sup> and Michael J. Pilling<sup>6</sup>

Received 28 July 2006; revised 10 October 2006; accepted 3 November 2006; published 31 March 2007.

[1] We use a continuous 6-year record (1996–2001) of GOME satellite measurements of formaldehyde (HCHO) columns over east and south Asia to improve regional emission estimates of reactive nonmethane volatile organic compounds (NMVOCs), including isoprene, alkenes, HCHO, and xylenes. Mean monthly HCHO observations are compared to simulated HCHO columns from the GEOS-Chem chemical transport model using state-of-science, “bottom-up” emission inventories from Streets et al. (2003a) for anthropogenic and biomass burning emissions and Guenther et al. (2006) for biogenic emissions (MEGAN). We find that wintertime GOME observations can diagnose anthropogenic reactive NMVOC emissions from China, leading to an estimate 25% higher than Streets et al. (2003a). We attribute the difference to vehicular emissions. The biomass burning source for east and south Asia is almost 5 times the estimate of Streets et al. (2003a). GOME reveals a large source from agricultural burning in the North China Plain in June missing from current inventories. This source may reflect a recent trend toward in-field burning of crop residues as the need for biofuels diminishes. Biogenic isoprene emission in east and south Asia derived from GOME is  $56 \pm 30 \text{ Tg yr}^{-1}$ , similar to  $52 \text{ Tg yr}^{-1}$  from MEGAN. We find, however, that MEGAN underestimates emissions in China and overestimates emissions in the tropics. The higher Chinese biogenic and biomass burning emissions revealed by GOME have important implications for ozone pollution. We find 5 to 20 ppb seasonal increases in surface ozone in GEOS-Chem for central and northern China when using GOME-derived versus bottom-up emissions. Our methodology can be adapted for other regions of the world to provide top-down constraints on NMVOC emissions where multiple emission source types overlap in space and time.

**Citation:** Fu, T.-M., D. J. Jacob, P. I. Palmer, K. Chance, Y. X. Wang, B. Barletta, D. R. Blake, J. C. Stanton, and M. J. Pilling (2007), Space-based formaldehyde measurements as constraints on volatile organic compound emissions in east and south Asia and implications for ozone, *J. Geophys. Res.*, *112*, D06312, doi:10.1029/2006JD007853.

### 1. Introduction

[2] Satellite measurements of formaldehyde (HCHO) columns offer “top-down” constraints to better quantify the emissions of reactive nonmethane volatile organic compounds (NMVOCs) with high spatial and temporal

resolution [Palmer et al., 2003a, 2006; Millet et al., 2006]. HCHO is a high-yield intermediate product from the oxidation of NMVOCs emitted by anthropogenic, biogenic, and biomass burning activities. NMVOCs are precursors of tropospheric O<sub>3</sub>, a major greenhouse gas and an important pollutant, and affect the concentration of OH radicals (the main tropospheric oxidant) in complicated ways [Houweling et al., 1998; Müller and Brasseur, 1999; Poisson et al., 2000]. NMVOCs can also condense to form secondary organic aerosols [Kanakidou et al., 2005], affecting radiation, cloud microphysics, and air quality.

[3] Long-term observations of HCHO columns from space are available from the Global Ozone Monitoring Experiment (GOME) satellite instrument launched in 1995 [Chance et al., 2000]. Previous analyses of these data have shown that HCHO column enhancements over North America in summer are mainly from the oxidation of biogenic isoprene and can be used quantitatively to estimate

<sup>1</sup>Department of Earth and Planetary Sciences and School of Engineering and Applied Sciences, Harvard University, Cambridge, Massachusetts, USA.

<sup>2</sup>School of Earth and Environment, University of Leeds, Leeds, UK.

<sup>3</sup>Now at School of GeoSciences, University of Edinburgh, Edinburgh, UK.

<sup>4</sup>Harvard-Smithsonian Center for Astrophysics, Cambridge, Massachusetts, USA.

<sup>5</sup>Department of Chemistry, University of California, Irvine, California, USA.

<sup>6</sup>Department of Chemistry, University of Leeds, Leeds, UK.

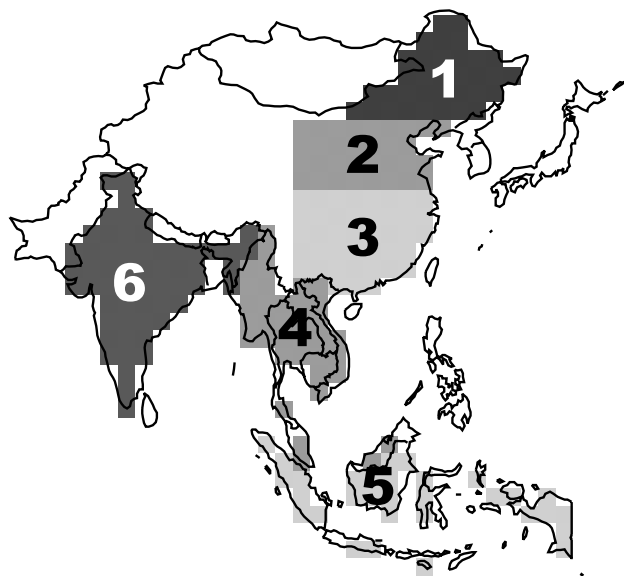


**Figure 1.** Geographical domain for the current study and coherent regions for which GOME constraints on NMVOC emissions are analyzed: (1) northeastern China, (2) northern China, (3) central and southern China, (4) Indochina, (5) Indonesia, and (6) India.

isoprene emissions with 40% uncertainty [Palmer *et al.*, 2001, 2003a, 2006; Abbot *et al.*, 2003; Millet *et al.*, 2006]. Meyer-Arnek *et al.* [2005] analyzed GOME HCHO columns over Africa in September 1997 and found major contributions from both biomass burning and biogenic sources. Shim *et al.* [2005] applied an inverse analysis to the GOME HCHO data to infer biogenic isoprene emissions, as well as biomass burning and industrial HCHO sources, in eight regions of the world. They derived a global biogenic isoprene emission of  $570 \text{ Tg C yr}^{-1}$ , compared to other global estimates ranging from  $250$  to  $750 \text{ Tg C yr}^{-1}$  [Wiedinmyer *et al.*, 2004; Guenther *et al.*, 2006].

[4] We use here the GOME HCHO column data as constraints on NMVOC emissions from east and south Asia (Figure 1). This is a region of particular interest because of the complex overlap between high anthropogenic, biogenic, and biomass burning emissions, none of which are well quantified at present. The most extensive regional inventory for anthropogenic and biomass burning emissions based on activity rates and emission factors (“bottom-up” approach) is that of Streets *et al.* [2003a]. They estimated NMVOC emissions for the domain of Figure 1 to be  $40 \text{ Tg yr}^{-1}$  from anthropogenic activities (including biofuel use) and  $12 \text{ Tg yr}^{-1}$  from biomass burning. The most extensive recent work for biogenic sources is that of Guenther *et al.* [2006], who combined satellite-derived land cover information and regional emission data to estimate a source of  $52 \text{ Tg yr}^{-1}$  isoprene for the domain in Figure 1. Although biogenic isoprene is the single largest NMVOC source according to the above inventories, it does not dominate in the manner that it does for North America [Palmer *et al.*, 2003a].

[5] Aircraft observations in Asian outflow have confirmed the Streets *et al.* [2003a] emission estimates for light alkanes [Carmichael *et al.*, 2003; Kurata *et al.*, 2004; Xiao

*et al.*, 2004], but cannot test the estimates for more reactive NMVOC species because of loss during transport. The inverse analysis of Shim *et al.* [2005] using GOME HCHO column data from September 1996 to August 1997 estimated a biogenic isoprene flux of  $77 \text{ Tg yr}^{-1}$  for east and south Asia. They also found a  $7 \text{ Tg yr}^{-1}$  reactive NMVOC source from biomass burning. Their analysis used coarse resolution and relatively old bottom-up emission inventories as prior information, which would affect the interpretation of spatial and temporal variability in the GOME data. We present here a more thorough analysis using (1) better spatial, temporal, and process resolution; (2) 6 years of updated GOME data processed with finer resolution; and (3) current state-of-science inventories as bottom-up constraints. We also examine the implications of our results for Asian ozone production.

## 2. Data and Model

### 2.1. GOME HCHO Vertical Columns for 1996–2001

[6] We use 1996 to 2001 measurements made by GOME, a nadir-scanning solar backscatter spectrometer aboard the ERS-2 satellite launched in April 1995 [European Space Agency, 1995; Burrows *et al.*, 1999]. The satellite is in a Sun-synchronous orbit, crossing the equator at 1030 local time (LT) in the descending mode. GOME has a surface spatial resolution of 40 km (along track) by 320 km (across track) and achieves global coverage every 3 days. HCHO “slant columns” along the optical path of the backscattered solar radiation are retrieved to  $4 \times 10^{15}$  molecule  $\text{cm}^{-2}$  uncertainty by directly fitting GOME radiance measurements at 337–356 nm [Chance *et al.*, 2000]. Recent laboratory comparisons showed that the HCHO cross sections used by Chance *et al.* [2000] may be too low, resulting in a possible 17% overestimate of HCHO retrieval (A. Gratien, personal communication, 2006).

[7] The reference solar irradiance measurements used for spectral fitting are taken by GOME approximately every three days, a period denoted as a “solar day.” The GOME diffuser plate is known to introduce error in these reference measurements, resulting in a global bias for all slant columns fitted using the reference solar spectrum from a given solar day [Richter and Wagner, 2001; Richter *et al.*, 2002]. In addition, occasionally there are “bad solar days” that feature large anomalies or discontinuities, and the frequency of these bad solar days increases in later years. Our procedure for data cleaning is detailed by Palmer *et al.* [2006]. We discard data from a particular solar day if the global mean HCHO slant column for that solar day (1) departs by more than one standard deviation from the global mean slant column for that month or (2) departs by more than  $5 \times 10^{16}$  molecule  $\text{cm}^{-2}$  from the global mean slant columns for the prior or next solar day. We then correct for the diffuser plate bias by removing the latitude-dependent differences between the GOME and GEOS-Chem model HCHO vertical columns over the remote Pacific for each solar day. Data from solar days without sufficient coverage over the remote Pacific are also discarded.

[8] HCHO slant columns are converted into actual vertical columns through the application of air mass factors (AMFs). The AMF is the ratio of the slant to the vertical column and is calculated with a radiative transfer model

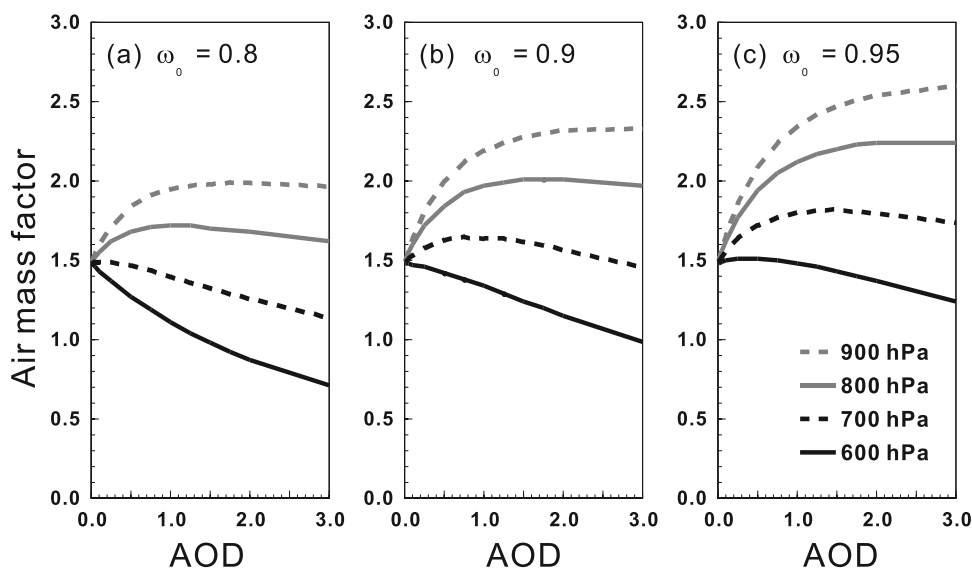


**Figure 2.** Sensitivity of the air mass factor (AMF) for HCHO retrievals to the aerosol optical depth (AOD), vertical distribution, and single scattering albedo ( $\omega_0$ ). In this calculation the surface pressure is 1000 hPa, surface albedo is 0.1, and solar zenith angle is  $25^\circ$ . The HCHO vertical profile of mixing ratio is assumed to be uniform up to 800 hPa and then decrease exponentially with altitude with a scale height of 2.7 km. The AOD is distributed vertically with uniform aerosol extinction coefficients from the surface up to 900 hPa (gray dashed), 800 hPa (gray solid), 700 hPa (black dashed), and 600 hPa (black solid).

[Spurr *et al.*, 2001] as a function of the viewing geometry, the scattering properties of the atmosphere and the surface, and the vertical distribution of HCHO (shape factor) [Palmer *et al.*, 2001]. We use local HCHO shape factors and aerosol scattering profiles from the GEOS-Chem chemical transport model [Palmer *et al.*, 2003a]. Surface UV albedo is based on GOME observations [Koelemeijer *et al.*, 2003]. Martin *et al.* [2004b] compared the resulting GOME HCHO columns with concurrent aircraft HCHO profiles over the southeastern United States. They found consistency within 20% in the mean. Millet *et al.* [2006] used a large ensemble of vertical HCHO profiles from the INTEX-A aircraft mission over eastern North America in summer 2004 to evaluate the AMF calculations done with GEOS-Chem. They found a mean bias and  $1\sigma$  uncertainty of  $<1\%$  and 15% for clear skies, increasing to 17% and 24% for scenes with 50% cloud cover, and inferred a general precision of 25–30% for the HCHO columns derived in this manner from the GOME data.

[9] We calculate here monthly averaged AMFs for the year 1997 and apply them to the entire study period. The year 1997 is chosen for its better data coverage compared to later years. Cloud fraction, cloud top, and cloud optical depths are retrieved for each GOME scene by the GOME Cloud AlgoriThm (GOMECAT) [Kurosu *et al.*, 1999]. We remove scenes with cloud fraction  $>40\%$ , following the recommendation of Millet *et al.* [2006]. This filter increases retrieved monthly mean HCHO concentrations by just 6%, so that the resulting clear-sky bias is small. Typical AMF values over land for our domain range from 0.7 to 1.0 in summer and 0.8 to 1.2 in winter. The daily variation with respect to the monthly mean AMF is less than 10% in summer and 15% in winter. Interannual variability is also weak. The difference between 1997 and 2001 monthly mean AMF is generally less than 30%, as previously

discussed by Palmer *et al.* [2006], supporting our use of 1997 monthly mean AMF values for the entire record.

[10] The aerosol effect on the AMF for biomass burning scenes warrants some discussion. In our standard calculations, the AMF for such scenes is in the low range ( $\sim 0.8$ ) because the biomass burning HCHO and aerosols have similar vertical profiles in GEOS-Chem, and backscattering by the biomass burning aerosol shields the underlying HCHO. Martin *et al.* [2003] reported a similar effect in their GOME retrievals of  $\text{NO}_2$ . We explored the sensitivity of the AMF to the aerosol optical depth (AOD), single-scattering albedo, and altitude relative to that of HCHO; results are shown in Figure 2. We find that the AMF is only moderately sensitive to AOD and single-scattering albedo, but highly sensitive to the differential altitude between HCHO and aerosols, increasing up to 2.5 when the aerosol layer is below the HCHO layer.

## 2.2. Inference of NMVOC Emissions From HCHO Column Data

[11] Palmer *et al.* [2003a] previously discussed the relationship between the HCHO columns observed by GOME and the underlying volatile organic compound (VOC) emissions. At steady state and in the absence of horizontal transport, the HCHO vertical column  $\Omega$  (molecule  $\text{cm}^{-2}$ ) would be linearly related to the sum of emissions of VOC precursors:

$$\Omega = \frac{1}{k_{\text{HCHO}}} \sum_i Y_i E_i, \quad (1)$$

where  $k_{\text{HCHO}}$  is the first-order HCHO loss rate constant from photolysis and oxidation applied to the HCHO column,  $E_i$  is the emission of VOC species  $i$ , and  $Y_i$  is the HCHO yield of that species.

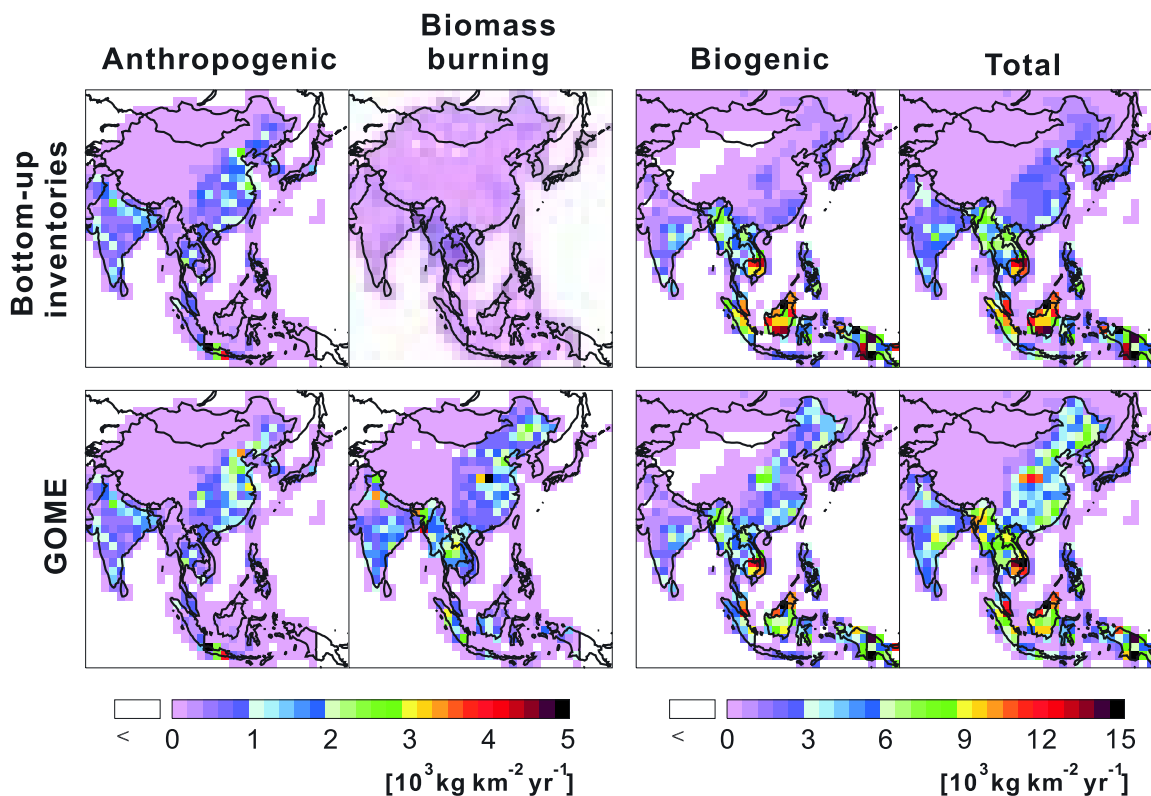


**Figure 3.** Annual mean reactive NMVOC emissions from east and south Asia. (top) Bottom-up inventories of *Streets et al.* [2003a] (anthropogenic, biomass burning) and *Guenther et al.* [2006] (biogenic). (bottom) Emissions inferred from GOME HCHO on the basis of the regression analysis from this study. Color scale at the left indicates anthropogenic and biomass burning, and the color scale on the right indicates biogenic and total sources.

[12] The lifetime of HCHO ( $\tau_{\text{HCHO}} = 1/k_{\text{HCHO}}$ ) is of the order of a few hours in the daytime, and the lifetimes of the VOCs against conversion to HCHO may range from less than an hour for isoprene under high- $\text{NO}_x$  conditions to 10 years for methane. Transport will thus smear the spatial relationship between HCHO column and VOC emission. *Palmer et al.* [2003a] defined a smearing length scale  $L_{s,i}$ , where the integral of  $\Omega$  downwind of the point of emission reaches  $(1 - 1/e) \sim 63\%$  of its asymptotic value. In the limit when the lifetime of VOC species  $i$  ( $\tau_i$ ) is much longer than the lifetime of HCHO,  $L_{s,i} \rightarrow U/\tau_i$ , where  $U$  is the relevant column wind speed. VOCs of very long lifetime, such as methane, yield a global HCHO background with no detectable localized signal. Assuming a  $U$  of  $5 \text{ m s}^{-1}$  and considering the GOME pixel length of 320 km, the signal from VOC species with lifetimes longer than  $320 \text{ km}/(5 \text{ m s}^{-1}) = 18 \text{ hours} \sim 1 \text{ day}$  is largely smeared from the GOME pixel where the species are emitted. Short-chain alkanes, benzene, ethyne, acetone, and methanol have lifetimes in excess of days and are largely smeared. Biogenic monoterpenes and methylbutenol and anthropogenic toluene have lifetimes typically less than a day, but their HCHO production is delayed because of long-lived intermediates and the resulting signals are also largely smeared [*Bloss et al.*, 2005a, 2005b; *Palmer et al.*, 2006]. Alkenes, isoprene, and xylenes have lifetimes shorter than a day, even in winter, and HCHO is produced promptly upon oxidation, so that smearing is minimal. We consider these, along with

directly emitted (primary) HCHO, as “reactive” NMVOCs since their emission should produce a local HCHO signal.

### 2.3. Bottom-Up Asian Emission Inventories of NMVOCs

[13] We use as starting point for our analysis the bottom-up NMVOC emission inventories of *Streets et al.* [2003a] for anthropogenic and biomass burning sources, and of *Guenther et al.* [2006] for biogenic sources. Figure 3 (top) shows the corresponding spatial distributions of reactive NMVOC emissions from each source type. Table 1 gives the total and reactive NMVOC emissions for six coherent regions and the entire domain of Figure 1. Table 2 gives the NMVOC speciation for each source type.

[14] The *Streets et al.* [2003a] anthropogenic inventory was developed using national and provincial (for China) statistics of activity levels for the year 2000, with spatial allocation on a  $1^\circ \times 1^\circ$  grid according to geographical features such as population, road network, land cover classes, etc. NMVOC emission factors were derived from western sources and sometimes adjusted for differences in performance [*Klimont et al.*, 2002]. The principal sources are residential combustion of coal and biofuel (34%) and transportation (27%) [*Streets et al.*, 2003a]. In addition to the major cities, emissions are also high in industrial eastern China, as well as in the Ganges valley and central India where biofuel is extensively used (Figure 3). *Streets et al.* [2003a] estimated a ratio of 1.5 between winter and summer NMVOC emissions in China reflecting the heating source. The total east and south Asian anthropogenic

**Table 1.** Reactive NMVOC Emissions<sup>a</sup> in East and South Asia<sup>b</sup>

Region	Bottom-Up			Top-Down <sup>f</sup>			Total
	Anthropogenic <sup>c,d</sup>	Biomass Burning <sup>d</sup>	Biogenic <sup>e</sup>	Anthropogenic <sup>c</sup>	Biomass Burning	Biogenic	
Region 1: northeastern China	0.46	0.15	0.91	0.57 ± 0.12	1.5 ± 0.53	4.1 ± 0.84	6.2 ± 1.0
Region 2: northern China	1.2	0.14	0.72	1.4 ± 0.3	1.8 ± 0.32	3.1 ± 0.48	6.3 ± 0.65
Region 3: central and southern China	1.9	0.29	2.4	2.3 ± 0.48	1.8 ± 0.38	5.5 ± 0.77	9.6 ± 0.98
Region 4: Indochina	1.0	0.79	13	1.0 ± 2.0 <sup>h</sup>	2.8 ± 0.95	13. ± 3.8	17. ± 4.4
Region 5: Indonesia	0.75	0.17	14	0.75 ± 1.5 <sup>h</sup>	1.9 ± 0.54	9.0 ± 1.5	12. ± 2.2
Region 6: India	2.5	0.56	5.9	2.5 ± 5.0 <sup>h</sup>	4.0 ± 0.73	6.0 ± 1.9	13. ± 5.4
Rest of east and south Asia <sup>g</sup>	3.1	1.1	15	3.1 ± 6.2 <sup>h</sup>	1.1 ± 3.3 <sup>h</sup>	15. ± 30. <sup>h</sup>	19. ± 31.
Domain total	11	3.2	52	12 ± 8.4	14. ± 3.6	56. ± 30	83. ± 32.

<sup>a</sup>Including alkenes, HCHO, xylenes, and isoprene (see section 2.2). The first three are mainly from anthropogenic and biomass burning sources; isoprene is from biogenic sources, as given in Table 2. Unit is Tg yr<sup>-1</sup>.

<sup>b</sup>Domain and regions defined in Figure 1.

<sup>c</sup>Biofuel use is included in the “anthropogenic” category.

<sup>d</sup>Streets *et al.* [2003a] for year 2000.

<sup>e</sup>Guenther *et al.* [2006].

<sup>f</sup>As derived from GOME HCHO observations (see text). Top-down uncertainties are represented by the standard deviation of the scaling factors in the regression analysis ( $\pm\sigma$ ). Bottom-up emission estimates and uncertainties are used where top-down constraints are not available. Total emission uncertainties are added in quadrature for each region. Additional top-down uncertainties not included in this estimate are (1) the previously derived uncertainty of 40% in inferring isoprene emission from GOME HCHO columns for individual scenes [Millet *et al.*, 2006], because that uncertainty is expected to decrease with averaging, and (2) the potentially large (up to a factor of 3) uncertainty for biomass burning scenes due to aerosols, because that uncertainty is difficult to quantify as discussed in the text and shown in Figure 2, and likely much less than a factor of 3.

<sup>g</sup>Domain in Figure 1 excluding regions 1–6.

<sup>h</sup>Top-down constraints not available. Bottom-up emission estimates are used; uncertainties are assumed to be a factor of 2 for anthropogenic and biogenic emissions, and a factor of 3 for biomass burning emissions (see text).

NMVOC emission given by Streets *et al.* [2003a] is 40 Tg yr<sup>-1</sup>, compared to 42 Tg yr<sup>-1</sup> estimated by the EDGAR 3.2 Fast Track 2000 data set (32FT2000) for the year 2000 [van Aardenne *et al.*, 2005]. Of the total anthropogenic NMVOC, 11 Tg yr<sup>-1</sup> is “reactive” as defined in section 2.2 and detectable by GOME, mostly consisting of ethene (40%) and higher alkenes (45%) (Table 2). Streets *et al.* [2003a] estimated a factor of 2 uncertainty in their total Asian anthropogenic NMVOC emissions.

[15] For biomass burning, Streets *et al.* [2003a] used annual burning reports at the country and provincial (China) level to represent average annual fire activity for the mid-1990s. They applied emission factors from Andreae and Merlet [2001], and spatially distributed the emissions on a 1° × 1° grid using Advanced Very High Resolution Radiometer (AVHRR) satellite fire counts and the Total Ozone Mapping Spectrometer (TOMS) aerosol index (AI) for 1999–2000. We compound this with a mean monthly variation of biomass burning emission from Duncan *et al.* [2003], which is based on the Along Track Scanning Radiometer (ATSR) satellite hot spot counts from 1996 to 2000. For February through April, monthly variation is specified following Heald *et al.* [2003] using calibrated AVHRR fire counts. The principal burning region given by Streets *et al.* [2003a] is Southeast Asia in spring (Figure 3), with the addition of weak emissions in eastern China (summer) and India (spring) from burning of agricultural residues [Streets *et al.*, 2003b]. Total biomass burning NMVOC emission for east and south Asia is 12 Tg yr<sup>-1</sup> in the Streets *et al.* [2003a] inventory, compared to 5.2 Tg yr<sup>-1</sup> from EDGAR 32FT2000 [van Aardenne *et al.*, 2005] for 1997–2001 average fire activity. Reactive NMVOC flux is 3.2 Tg yr<sup>-1</sup>, consisting of approximately equal fractions of ethene, higher alkenes, and HCHO (Table 2). Streets *et al.* [2003a] estimate a factor of 3 uncertainty in total Asian NMVOC biomass burning emissions.

[16] Biogenic emissions are described by the MEGAN inventory [Guenther *et al.*, 2006], which includes major

updates and new data relative to the previous GEIA inventory of Guenther *et al.* [1995]. Isoprene base emissions are specified for different vegetation types and then mapped on the basis of vegetation cover derived from the MODIS satellite instrument [Strahler *et al.*, 1999]. The MEGAN inventory is implemented in GEOS-Chem as described by Palmer *et al.* [2006], including dependences on local temperature and solar radiation. Leaf area index (LAI) from AVHRR [Myneni *et al.*, 1997] is used to determine the seasonal start and shutdown of vegetation growth. Biogenic emission of propene and 1-butene is small and scaled to 2.9% of total biogenic isoprene following Goldstein *et al.* [1996].

[17] East and south Asian isoprene flux is 52 Tg yr<sup>-1</sup> in MEGAN, not much different from the 60 Tg yr<sup>-1</sup> in GEIA. However, the spatial distributions in the two inventories are very different. More than 50% of the Asian biogenic isoprene in MEGAN is from broadleaf evergreen forests

**Table 2.** Speciated East and South Asia<sup>a</sup> NMVOC Emissions From Bottom-Up Inventories<sup>b</sup>

	Anthropogenic <sup>c</sup>	Biomass Burning <sup>c</sup>	Biogenic	Total
Reactive NMVOCs				
Ethene	4.4	1.2	...	5.6
Other alkenes	4.8	1.0	1.6 <sup>d</sup>	7.4
HCHO	0.4	1.0	...	1.4
Isoprene	...	...	52 <sup>e</sup>	52
Xylenes	1.2	0.042	...	1.2
Other NMVOCs <sup>f</sup>	29	8.7	26 <sup>g</sup>	64
Total NMVOCs	40	12	80	130

<sup>a</sup>Domain defined in Figure 1.

<sup>b</sup>Unit is Tg yr<sup>-1</sup>.

<sup>c</sup>Streets *et al.* [2003a] for year 2000.

<sup>d</sup>Includes biogenic propene and 1-butene; their emission is assumed 2.9% of that of isoprene following Goldstein *et al.* [1996].

<sup>e</sup>Guenther *et al.* [2006].

<sup>f</sup>Including alkanes, ethyne, ketones, monoterpenes, methanol, benzene, toluene, and other aromatics.

<sup>g</sup>Includes 19 Tg yr<sup>-1</sup> monoterpenes (A. Guenther, unpublished data, 2005), 6.6 Tg yr<sup>-1</sup> acetone [Jacob *et al.*, 2002], and 0.24 Tg yr<sup>-1</sup> methanol [Jacob *et al.*, 2005].

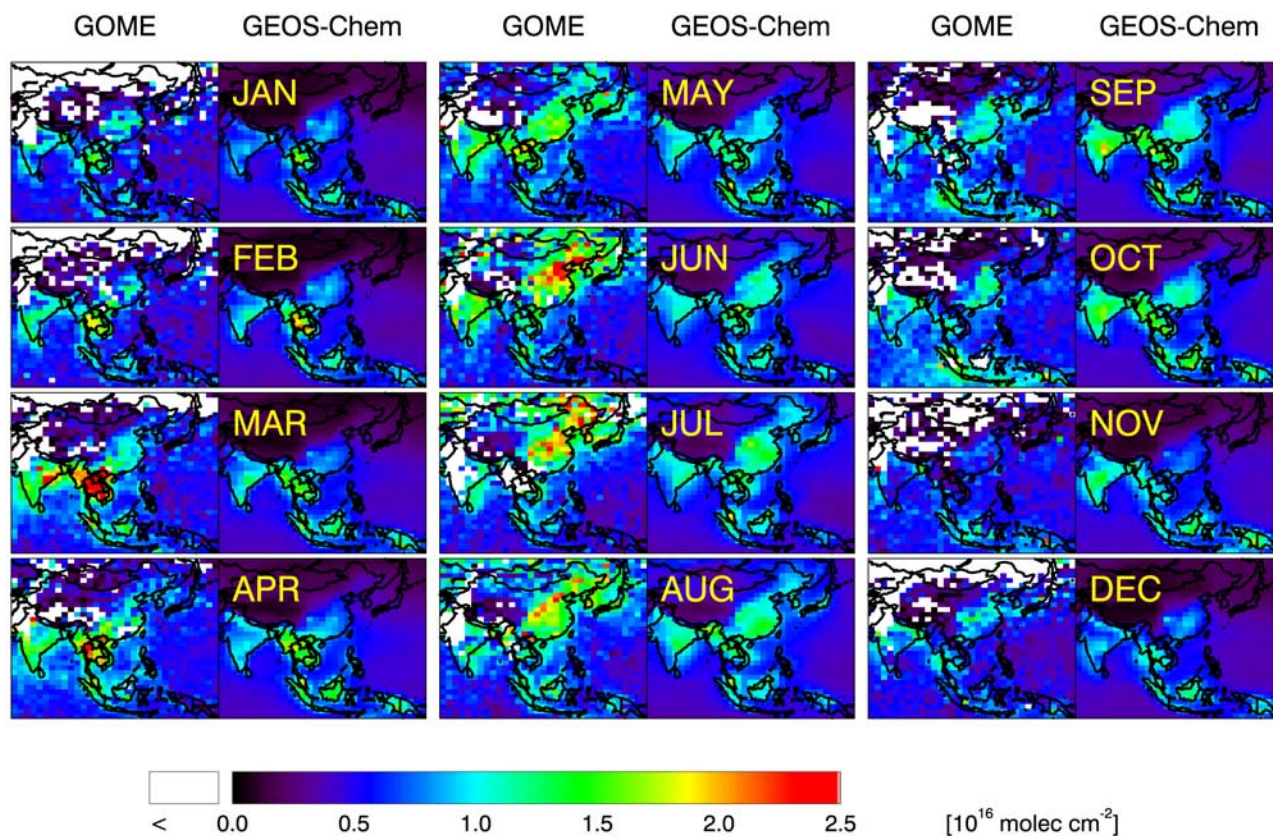


**Figure 4.** Monthly mean HCHO columns over Asia as observed by GOME from 1996 to 2001 (left plots in each column) and as simulated by GEOS-Chem for 2001 (right plots in each column). The GEOS-Chem simulation uses the bottom-up emission inventories described in section 2.3 and shown in Figure 3 (top). Model results are sampled between 0900 and 1200 LT. GOME observations are at about 1030 LT. The color scale is capped at  $2.5 \times 10^{16}$  molecule  $\text{cm}^{-2}$  to emphasize features. Peak GOME observations over Southeast Asia in March and over the North China Plain in June are as high as  $3.0 \times 10^{16}$  molecule  $\text{cm}^{-2}$ .

in Indonesia and Indochina (Figure 3); whereas this contribution was only 30% in the GEIA inventory. Steiner *et al.* [2002] calculated biogenic emissions for east Asia (eastern China and northern Indochina), using ecosystem-dependent emission factors from Guenther *et al.* [1995] and land cover data from AVHRR. They estimated an isoprene flux of  $13.6 \text{ Tg yr}^{-1}$ , falling between the estimates for the same region from MEGAN ( $10.8 \text{ Tg yr}^{-1}$ ) and GEIA ( $19.7 \text{ Tg yr}^{-1}$ ). We thus estimate that the uncertainty in regional biogenic isoprene emissions is about a factor of 2.

#### 2.4. GEOS-Chem Model

[18] We use the GEOS-Chem global 3-D chemical transport model (version 7.1.2; <http://www-as.harvard.edu/chemistry/trop/geos/>) to provide HCHO shape factors and aerosol vertical profiles for the AMF calculation (section 2.1) and to simulate the relationship between HCHO columns and emissions of NMVOC precursors. The model is driven by assimilated meteorology for the year 2001 from the Goddard Earth Observing System (GEOS-3) of the NASA Global Modeling Assimilation Office [Bey *et al.*, 2001]. The meteorological data are updated every 3 hours for surface variables and every 6 hours for other variables with a resolution of  $1^\circ$  latitude  $\times$   $1^\circ$  longitude horizontally and 48 sigma levels vertically up to 0.1 hPa. For driving

GEOS-Chem simulations, we regrid the horizontal resolution to  $2^\circ$  latitude  $\times$   $2.5^\circ$  longitude.

[19] GEOS-Chem contains a detailed  $\text{O}_3$ - $\text{NO}_x$ -VOC-aerosol chemical mechanism [Horowitz *et al.*, 1998; Bey *et al.*, 2001; Martin *et al.*, 2003; Park *et al.*, 2004]. It has been used in several previous studies to interpret GOME data for HCHO [Palmer *et al.*, 2001, 2003a, 2006; Abbot *et al.*, 2003; Shim *et al.*, 2005],  $\text{NO}_2$  [Martin *et al.*, 2002, 2003, 2006; Jaeglé *et al.*, 2004, 2005], and tropospheric ozone [Liu *et al.*, 2006]. The model has also been used previously for constraining Asian sources of CO,  $\text{NO}_x$ , methane, ethane,  $\text{CO}_2$ , and aerosols through simulations of aircraft observations in Asian outflow [Palmer *et al.*, 2003b; Suntharalingam *et al.*, 2004; Y. X. Wang *et al.*, 2004; Xiao *et al.*, 2004; Park *et al.*, 2005] and MOPITT satellite observations for CO [Heald *et al.*, 2004; Arellano *et al.*, 2004; Turquety *et al.*, 2007]. Hydrocarbons in the standard GEOS-Chem chemical mechanism include methane, ethane, propane,  $>\text{C}_3$  alkanes,  $>\text{C}_2$  alkenes, isoprene, and monoterpenes. For this work we expanded the mechanism to include ethene and xylenes in view of their potential importance as sources of HCHO in Asia. The oxidation mechanism of ethene is taken from the Master Chemical Mechanism (MCM) version 3 [Saunders *et al.*, 2003], with OH being the main oxidant and yielding 0.89 HCHO per C

reacted under high  $\text{NO}_x$  conditions. The oxidation of xylenes by OH is assumed to produce instantaneously 0.24 HCHO per C reacted, on the basis of detailed calculations from MCM version 3.1 under high  $\text{NO}_x$  conditions [Bloss *et al.*, 2005a, 2005b].

[20] We performed a 1-year full-chemistry simulation for 2001 with the emission inventories described in section 2.3. The model was initialized for six months with a July–December 2001 simulation, and then restarted to run from January through December 2001. The sensitivity of HCHO columns to each source type are determined by perturbing by 30% the respective emissions of reactive NMVOCs.

### 3. Regional and Seasonal Patterns of GOME HCHO Columns

[21] Figure 4 shows the 1996 to 2001 composite monthly mean HCHO vertical columns observed by GOME and compares them with the GEOS-Chem simulation using the bottom-up emission inventories. Model results are averaged between 0900 and 1200 LT. The observed HCHO seasonal variation is much stronger than the interannual variation of emissions. *Streets et al.* [2003a] estimate that anthropogenic NMVOC emissions increased by 8–11% in east and south Asia between 1995 and 2000. *Heald et al.* [2003] report that the interannual variability of fire activity in Southeast Asia (the principal burning region) is 20%, and that activity level for 1997–2001 was 20% lower than the 1979–2001 mean.

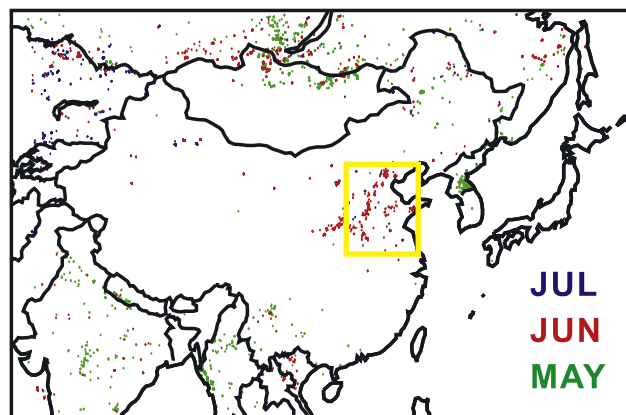
[22] The most prominent feature in the model results of Figure 4 is the seasonal maximum over China in summer due to biogenic emissions. The model HCHO is also enhanced from February to April over Indochina because of biomass burning. Over India, HCHO peaks in the model in September when high temperatures and insolation produce a seasonal maximum of isoprene emission. In extratropical winter when biogenic and biomass burning emissions are absent, the model still produces large anthropogenic HCHO signals in urban areas of central and southern China including Chongqing, Changsha, Wuhan, and Guangzhou.

[23] The GOME HCHO observations in Figure 4 show a number of discrepancies with the model. In winter, HCHO columns are significantly larger than the model in China, especially over major cities including Beijing, Jinan, Shanghai, Zhengzhou, Changsha, Wuhan, Chongqing, Guangzhou, and along the Yangtze River, indicating greater anthropogenic emissions. High HCHO is also observed over the biofuel-burning Ganges valley and central India, as well as major Indian cities including Mumbai and Bangalore. Over Indonesia, observed November–February HCHO columns are smaller than the modeled HCHO, which is dominated by biogenic emissions.

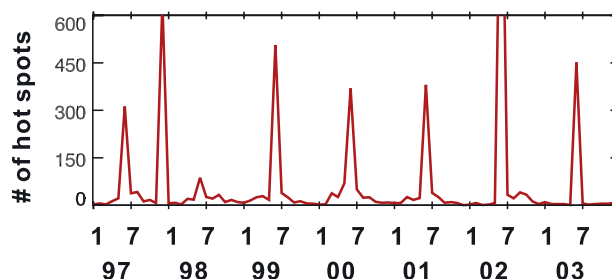
[24] From February to April, GOME HCHO columns are higher than the model over the biomass burning region of Indochina and India but lower over Indonesia. Over southern China, GOME shows HCHO columns greater than  $1 \times 10^{16}$  molecule  $\text{cm}^{-2}$  as early as March. These high HCHO columns expand northward to northeastern China as the summer progresses, finally shutting down in October, consistent with a biogenic emission pattern.

[25] In June, GOME observes HCHO columns exceeding  $2.5 \times 10^{16}$  molecule  $\text{cm}^{-2}$  over extensive parts of the North

#### (a) Summer 1997 ATSR hot spots



#### (b) ATSR hot spots 1997 - 2003 North China Plain



#### (c) Winter Wheat Harvest

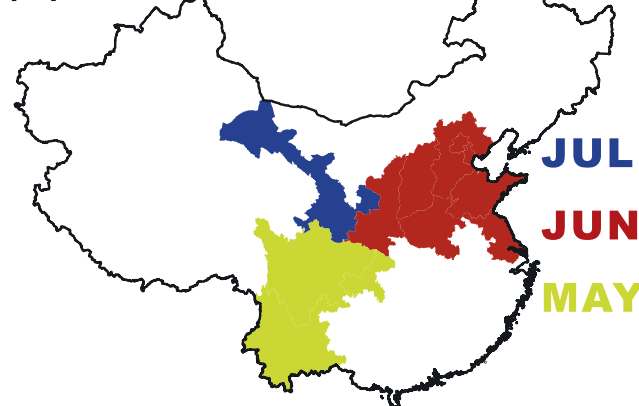


**Figure 5.** Evidence for large agricultural biomass burning in the North China Plain in June. (a) ATSR hot spots over China for May–July 1997; (b) ATSR monthly hot spot counts time series over the North China Plain (yellow box) for 1997–2003; and (c) spatial extent and timing of winter wheat harvest in China, based on data from *Ministry of Agriculture of China* [2007].

China Plain (NCP) and northeastern China, but this is not seen in the model. These high HCHO features recur annually through the 6 years of observation, and their timing and spatial extents coincide with the local fire activity. Figures 5a and 5b show the ATSR hot spots in summer 1997 and monthly hot spot counts from 1997 to 2003 over the NCP.

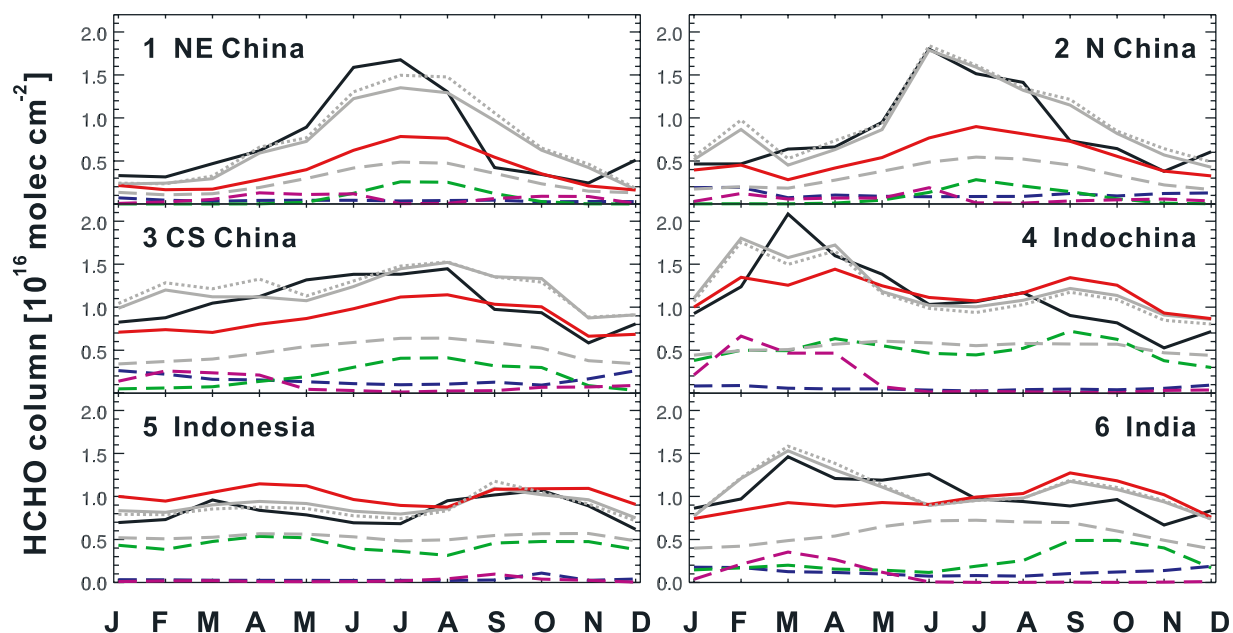


**Figure 6.** Monthly mean HCHO vertical columns averaged over each region of Figure 1. GOME observations from 1996 to 2001 (black solid) are compared to modeled HCHO columns on the basis of the bottom-up inventories of Figure 3 (red solid). Background HCHO (simulated by shutting off all reactive Asian NMVOC emissions) is shown as grey dashed lines, and the difference with the red line represents the enhancement due to regional sources. The contribution of each source to this regional HCHO enhancement is shown as dashed lines: anthropogenic (blue dashed), biogenic (green dashed), and biomass burning (3X, purple dashed). Also shown are the HCHO columns calculated in the GEOS-Chem model using the GOME-inferred emissions as shown in Figure 3 (grey solid) and the linear extrapolation of HCHO enhancements based on the regression model equation (2) (grey dotted).

These fire activities correspond with the local harvest of winter wheat from June to early July (Figure 5c). We hypothesize that the observed high HCHO columns are produced by crop residue burning after the harvest.

[26] Indirect evidence of extensive biomass burning over the NCP in June can be found in several previous studies. Duan *et al.* [2001] measured the  $K^+$  concentration (biomass burning tracer) in particulate matter collected outside Beijing and found the concentrations in June 1998 to be three times those in May or July 1998. MODIS AOD measurements also show recurring peaks in June over this region (not shown). Measurements at a rural central China site found the  $CO/NO_y$  concentration ratio to peak in June and October [T. Wang *et al.*, 2004], the latter likely associated with the rice harvest.

[27] Between September and November, GOME HCHO columns are lower over Southeast Asia and India than in the model, where they are dominated by biogenic emissions. Both the observed and simulated HCHO columns are notably low in China in November, possibly because the biogenic emissions are shut off while the anthropogenic emissions have not yet significantly increased. The official winter heating period in many major Chinese cities, including Beijing, starts 15 November and ends 15 March.

[28] To further examine the seasonal differences between the GOME observations and the model simulations, we selected from the domain of Figure 1 six regions where GOME has significant regional enhancements and good spatial coverage. These include northeastern China, north-

ern China, central and southern China, Indochina (Burma, Cambodia, Laos, Malaysia, Thailand, and Vietnam), Indonesia, and India (Figure 1). We do not examine Japan, South Korea, or the Philippines because there are too few GOME pixels to provide adequate characterization.

[29] Figure 6 shows the 1996 to 2001 monthly areal averages of GOME HCHO vertical columns for each of the six regions. Also shown are the corresponding GEOS-Chem simulation, the simulated background HCHO (HCHO columns when all Asian reactive NMVOC emissions are shut off), and the modeled enhancement of HCHO columns due to reactive NMVOC anthropogenic, biomass burning, and biogenic emissions, approximated by multiplying the sensitivity coefficients derived from section 2.4 by the corresponding bottom-up emissions. This approximation neglects nonlinear effects on photochemistry but these are small, as discussed in section 5.

[30] We find in GEOS-Chem that 30% to 60% of the total HCHO column for each region of Figure 1 is due to reactive NMVOC emissions from within the region. The seasonal variation of these regional enhancements, indicated by the difference between total model HCHO (red solid lines) and model background (grey dashed lines) shows a prominent contribution from biogenic emissions. Model HCHO peaks in July and August over China, in April and September over Indochina and Indonesia, and in September over India. HCHO enhancement associated with biomass burning is significant only from February to April over Indochina and India; even there its magnitude is only half of the HCHO

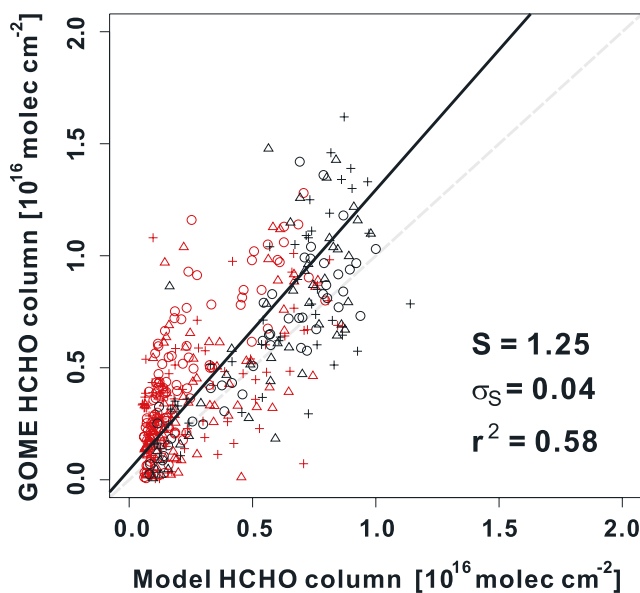


**Figure 7.** Chinese wintertime HCHO columns observed by GOME (1996–2001) versus GEOS-Chem model results. Individual points correspond to the model  $2^\circ \times 2.5^\circ$  grid over China from Figure 4 for December (circles), January (triangles), and February (pluses), north of  $30^\circ\text{N}$  (red) and south of  $30^\circ\text{N}$  (black). The thick black line indicates the reduced major axis regression [Hirsch and Gilroy, 1984]; the corresponding slope ( $S$ ), standard deviation of slope ( $\sigma_S$ ), and correlation ( $r^2$ ) are shown inset. The grey dashed line is the 1:1 ratio.

enhancement from biogenic emissions. HCHO enhancement from anthropogenic sources is largest in winter months, reflecting the stronger heating source. In China, HCHO enhancements due to biomass burning and biogenic emissions are very small during the winter months, hence anthropogenic sources dominate. Although anthropogenic emission is also large in India, it does not dominate in any season as biogenic emission is significant throughout the year.

[31] Observed HCHO columns over China are significantly larger than those in the model in spring, summer, and winter. Over northeastern China, observed high HCHO from late spring to early summer suggests a large model underestimate of biomass burning. The HCHO maximum in northern China in June appears to be due to agricultural burning following the winter wheat harvest, as discussed above. Aside from this agricultural burning signal, the summertime enhancement in the GOME HCHO columns over China in summer is likely due to biogenic emissions, and these are much higher than in the model. GOME and GEOS-Chem agree well in fall when biogenic emissions shut off. In winter, although GOME only features a slight regional HCHO enhancement, its spatial distribution as shown in Figure 4 demonstrates its association with anthropogenic activities.

[32] GOME HCHO over Southeast Asia and India is consistently higher than the model in March and lower than the model in fall, implying an underestimate of springtime biomass burning and an overestimate of biogenic emissions. A similar situation is observed over Indonesia, where

observed and modeled HCHO enhancements are similar in magnitude but the model lags by 1 month.

#### 4. Constraints on Anthropogenic VOC Emissions in China

[33] Over China, both biogenic and biomass burning emissions shut down in winter; therefore the observed HCHO enhancements can be attributed to anthropogenic sources. Figure 7 shows the correlation of 1996–2001 monthly mean GOME and model HCHO columns for December, January, and February for all Chinese  $2^\circ \times 2.5^\circ$  model grid points in Figure 4. The model captures 58% of the spatial variance in the observations, but the observations are +25% larger, with a 95% confidence interval of +19% to +35% (jackknife estimation). Increasing the Streets *et al.* [2003a] estimate of anthropogenic reactive NMVOC emissions by 25% results in an improved top-down estimate of Chinese reactive NMVOC emissions of  $4.5 \pm 0.74 \text{ Tg yr}^{-1}$ . The slope of the regression in Figure 7 does not change significantly if we distinguish between Chinese grid points north and south of  $30^\circ\text{N}$ . Thus the +25% bias is unlikely to be caused by incorrect seasonal variation of the heating source.

[34] Inverse analysis by Shim *et al.* [2005] found the industrial reactive NMVOC sources from east Asia (China, Korea, and Japan) to be  $7 \text{ Tg yr}^{-1}$ , larger than our estimate of  $5 \text{ Tg yr}^{-1}$ . However, theirs is not a robust estimate, since for the data used in their analysis over east Asia (May to August 1997), anthropogenic emissions contribute less than 5% of the total HCHO column, much smaller than the variation of either biogenic or biomass burning sources. Their use of a  $4^\circ \times 5^\circ$  resolution grid would further contribute to diluting the anthropogenic signal.

[35] Further insight into the cause of the anthropogenic emission underestimate can be gained from in situ NMVOC and CO concentration data collected by Barletta *et al.* [2005] in 43 Chinese cities (158 canisters total) in January–February 2001. Concentrations are extremely high in these samples, reflecting the dominance of local emissions. They average 2300 ppb CO, 7.2 ppb ethane, 3.9 ppb propane, 3.7 ppb butane, 5.0 ppb pentane, 11 ppb ethene, 2.4 ppb propene, 14 ppb ethyne, 2.5 ppb benzene, 3.4 toluene, and 4.9 ppb total xylenes. Taking CO as a reference species for anthropogenic emissions, we can compare the NMVOC to CO concentration ratios in the Barletta *et al.* [2005] data to the local emission ratios from Streets *et al.* [2003a] inventory after adjusting the CO emission totals on the basis of inverse modeling of MOPITT satellite observations [Heald *et al.*, 2004]. Figure 8 compares the resulting emission ratios to the Barletta *et al.* [2005] observations for selected species. At the 95% significance level, the emission ratios are too high for ethene, propene, benzene, and toluene, and too low for pentane and xylenes. In China, most of the anthropogenic emission of ethene, propene, and benzene comes from stationary combustion, while toluene is from paint use (45%), transportation (25%) and stationary combustion (20%) [Klimont *et al.*, 2002]. In particular, more than half of the anthropogenic ethene is associated with biofuel burning [Streets *et al.*, 2003a]. More than 50% of the anthropogenic emission of pentane and xylenes is due to transportation, with smaller contributions from stationary combustion (27% of xylenes), extraction

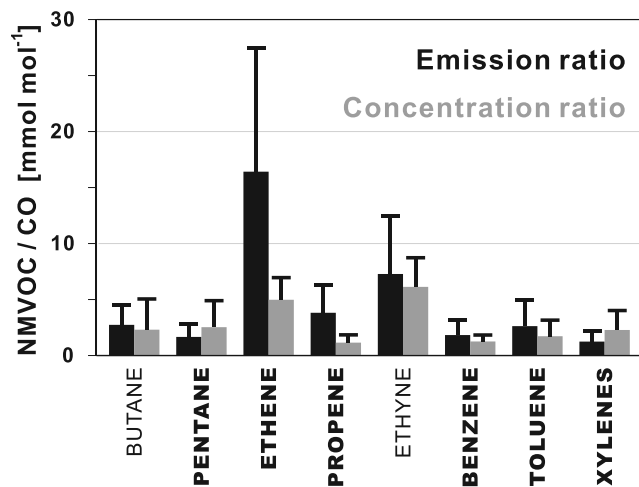


**Figure 8.** NMVOC/CO molar concentration ratios (in grey) measured by Barletta et al. [2005] in 43 Chinese cities in January-February 2001, compared to the corresponding local emission ratios (in black) from the Streets et al. [2003a] inventory with CO emissions adjusted according to Heald et al. [2004]. Shown are mean values and standard deviations ( $n = 43$ ). Species with name boldfaced have mean concentration ratio and mean emission ratio different at the 95% significance level.

and processing (16% of pentane), and paint use (15% of pentane). The 25% underestimate of anthropogenic NMVOC emissions in the Streets et al. [2003a] inventory apparent from the GOME data is therefore likely due to transportation emissions.

[36] One possibility is that Chinese vehicles may be large primary sources of HCHO. Kolb et al. [2004] found that the HCHO/CO<sub>2</sub> emission ratio from vehicles in Mexico City is an order of magnitude larger than that in Boston, for reasons that were not identified. Measurements of wintertime HCHO in Seoul by Lee et al. [2005] indicate major primary emissions from vehicle exhaust and heating burners. Streets et al. [2003a] assume in their inventory a low HCHO/CO<sub>2</sub> emission ratio typical of vehicles in the United States; if it were an order of magnitude larger, our simulated wintertime HCHO columns would increase by 10%, possibly accounting for part of the discrepancy between GOME and the model.

## 5. Constraints on Biogenic and Biomass Burning Emissions

[37] For each region of Figure 1, the relationship between the mean observed HCHO column ( $\Omega$ ) and the regional emissions  $E_i$  (where  $i = 1, 3$  describes anthropogenic, biomass burning, and biogenic sources) can be expressed with a Taylor-type equation,

$$\Omega = \Omega_0 + \sum_{i=1}^3 \frac{\partial \Omega}{\partial E_i} \cdot E_i + \text{nonlinear terms}, \quad (2)$$

where  $E_i$  is the regional reactive NMVOC emission flux of source type  $i$ .  $\partial \Omega / \partial E_i$  is the HCHO sensitivity to  $E_i$  as

calculated with the model (section 2.4), and  $\Omega_0$  is the background HCHO due to long-lived VOCs which we assume is well simulated by the model. Nonlinearity in equation (2) reflects the OH source from HCHO photolysis but the effect is small, as will be demonstrated. Figure 6 shows  $\Omega_0$  for each region, as well as  $\partial \Omega / \partial E_i$  scaled by the bottom-up emission estimates of reactive NMVOCs (Table 2). The assumption of correct background is appropriate for two reasons. First, the GOME observations are debiased by forcing the observed HCHO vertical columns to match model values over the remote Pacific. Second, previous analysis of TRACE-P measurements in Asian outflow showed that the emission of longer-living alkanes in the Streets et al. [2003a] inventory is not significantly biased [Carmichael et al., 2003; Kurata et al., 2004; Xiao et al., 2004].

[38] For each region, we use a linear regression to fit the GOME HCHO monthly mean column (Figure 6) to the seasonal sensitivity from each source type, ( $\partial \Omega / \partial E_i$ ), assuming that the relative seasonal variations for each source type from the bottom-up inventories are correct. There should be little error in these relative seasonal variations since they are largely constrained by satellite observations of leaf area index for biogenic emissions and fire hot spots for biomass burning emissions. The scaling factors from the linear regression yield the top-down estimates of reactive NMVOC emissions for the region as constrained by the GOME data; the standard deviation of the scaling factors represent top-down estimate uncertainties. In practice we only fit for the biogenic and biomass burning emissions, which dominate the seasonal variation of the monthly mean data in Figure 6. The anthropogenic term for the Chinese regions was previously constrained on the basis of the wintertime GOME data to be 25% larger than the bottom-up inventory, and is otherwise a weak term that cannot be reliably fitted. We performed a lack-of-fit test using  $F$ -statistics and found that including the anthropogenic term did not significantly improve the regression. Figure 6 also compares the HCHO columns modeled with full chemistry using GOME-inferred emissions to that extrapolated linearly using regression results. For all six regions, the difference due to OH nonlinearity is generally less than 5% and always less than 20%. Further feedback mechanisms, such as the effect of atmospheric aerosols on crop growth [Chameides et al., 1999], are not considered.

[39] Table 1 summarizes the top-down estimates for biogenic and biomass burning emission fluxes from the regression. For all six regions, the linear regression model explains 80% to 90% of the seasonal variance in the GOME monthly mean HCHO columns. Biogenic isoprene fluxes from east and south Asia inferred from GOME are  $56 \pm 30 \text{ Tg yr}^{-1}$ , slightly larger than the  $52 \text{ Tg yr}^{-1}$  from the MEGAN inventory. There are however great regional differences, as illustrated in Figure 3. The top-down estimates are 2 to 5 times the emission from MEGAN for the mixed forests and croplands in China, but 40% less than MEGAN for the evergreen broadleaf forests in Indonesia. Over Indochina and India, the top-down estimates are similar to the MEGAN inventory. The uncertainty of the total top-down estimate is  $\pm 30 \text{ Tg yr}^{-1}$ , calculated by combining the top-down uncertainties in quadrature and assuming the

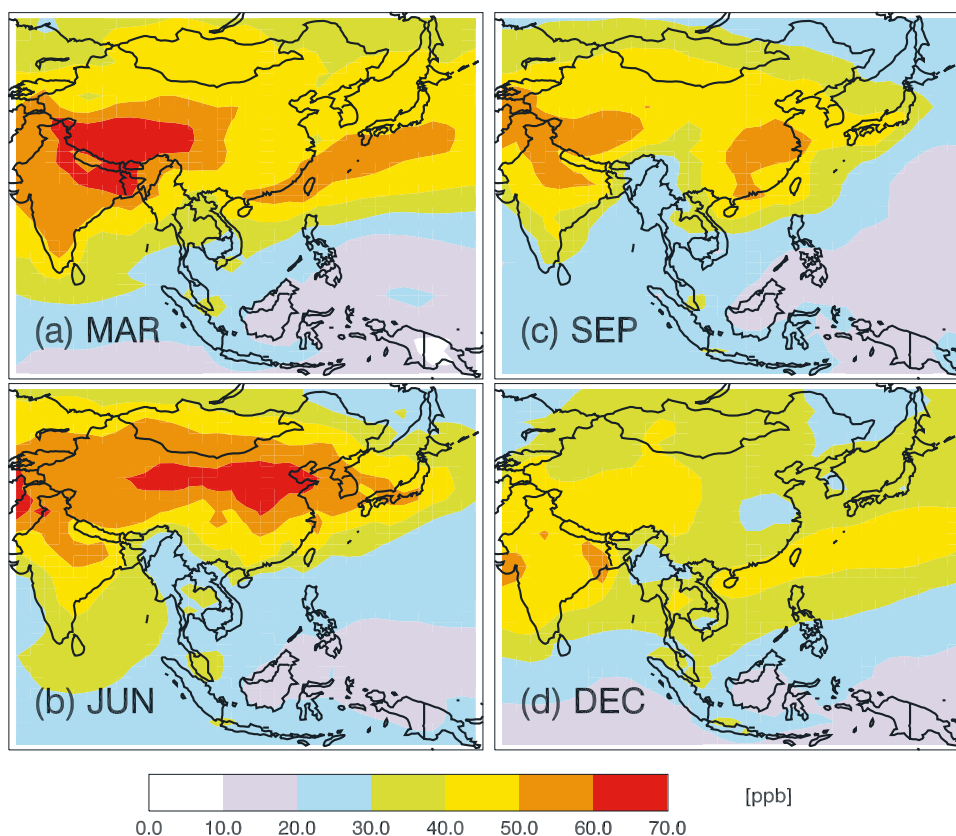


**Figure 9.** Monthly mean afternoon (1300 to 1700 LT) surface ozone concentrations simulated by GEOS-Chem using bottom-up inventories for NMVOCs (section 2.3) in (a) March, (b) June, (c) September, and (d) December 2001.

bottom-up uncertainties where emissions are not constrained by GOME.

[40] GOME observations imply remarkably large biomass burning emissions of reactive NMVOCs throughout east and south Asia,  $14 \pm 3.6 \text{ Tg yr}^{-1}$  versus  $3.2 \text{ Tg yr}^{-1}$  in the *Streets et al.* [2003a] inventory (Figure 3). The ratios of top-down to bottom-up estimates are 6 to 13 over China, 11 over Indonesia, and 7 over India. The smallest enhancement is over Indochina; even there the GOME-inferred emission is 3.6 times the bottom-up estimate.

[41] We previously pointed out in section 2.2 that errors in the AMF calculation due to smoke aerosols could possibly cause a GOME overestimate of HCHO vertical columns in biomass burning scenes by up to a factor of 3. However, the observed discrepancies with the bottom-up estimates are larger. Therefore the bottom-up inventory must underestimate the amount of biomass available, the fraction of biomass burned, the emission factors for reactive NMVOCs, or a combination thereof. An inverse study of MOPITT CO by *Heald et al.* [2004] for March–April 2001 inferred a biomass burning CO emission of  $45 \text{ Tg yr}^{-1}$  for Indochina, as compared to  $20 \text{ Tg yr}^{-1}$  in the work by *Streets et al.* [2003a], also suggesting an underestimate. To our knowledge, the only direct measurements of NMVOC and CO emission factors for Asian biomass are those by *Christian et al.* [2003]; they found CO and HCHO emission factors for Indonesian grass, shrub, and rice straw to be 2–3 times larger than those of *Andreae and Merlet* [2001]

used by *Streets et al.* [2003a]. Underestimate of CO emissions might be expected to be linked to an underestimate of NMVOC emissions, as both are emitted in greater quantity from wet biomass or incomplete, smoldering combustion [*Korontzi et al.*, 2003]. Recent analysis over the tropics also found GEOS-Chem HCHO columns over biomass burning regions to be low by more than a factor of two, compared to GOME observations [*Sauvage et al.*, 2007].

[42] A remarkable result is the large biomass burning emission deduced from the GOME observations over the NCP in June. We previously identified this as the burning of crop residues following the winter wheat harvest, which is included in the *Streets et al.* [2003a] inventory but with very low emission. The amount of crop residue estimated by *Streets et al.* [2003a] is consistent with Chinese official statistics of crop production [*National Bureau of Statistics*, 2000], and is therefore not likely to be grossly in error. *Streets et al.* [2003a] assumed the fraction of crop residue burned in field to be 17%, on the basis of *Hao and Liu* [1994]. Much anecdotal evidence suggest that this fraction has increased over the past decade as farmers turn to commercial sources for fuel, animal feed, and fertilizers (R. Yevich, personal communication, 2005). Recent work by *Cao et al.* [2005a, 2005b] assumed that 50% of the crop residue is burned in field. Yet another factor to consider is that the wet season in the NCP starts in June, and Chinese wheat is planted very densely, so combustion would be

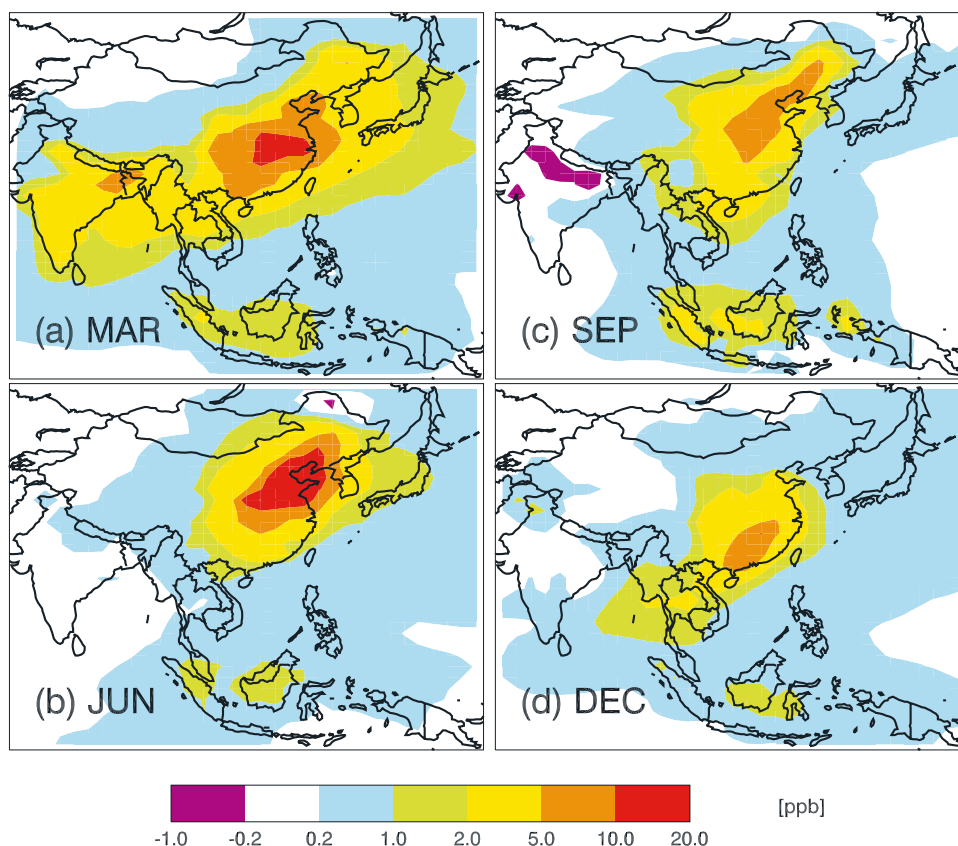


**Figure 10.** Difference in modeled monthly mean afternoon (1300 to 1700 LT) surface ozone concentrations using GOME-inferred reactive NMVOC emission versus the bottom-up inventories for (a) March, (b) June, (c) September, and (d) December 2001.

incomplete and smoldering. It is likely that the NMVOC emission factors would be high under these conditions.

[43] Rice is harvested in southern China during the fall months. However, we do not see a corresponding large biomass burning signal from GOME HCHO columns. Satellite instruments do detect fires in this region during the fall [Guo *et al.*, 2006], but the ATSR fire counts are far less than those detected over the NCP in June. We speculate that the lack of strong biomass burning emissions from rice harvesting might be due to different farming practice for the crops. Also, it is possible that farmers have more incentive to store the crop residue as biofuel as winter draws near. Systematic survey and measurements are clearly needed to better understand this emission from crop residue burning.

## 6. Implication for Ozone Simulation in Asia

[44] The Asian reactive NMVOC emissions inferred above from GOME significantly impact regional simulations of ozone pollution. Figure 9 shows the GEOS-Chem monthly mean afternoon (1300 to 1700 LT) surface  $O_3$  concentration simulated using the bottom-up NMVOC emission inventories described in section 2.3.  $NO_x$  emissions are given by Streets *et al.* [2003a], with adjustments from a GEOS-Chem inverse analysis by Y. X. Wang *et al.* [2004]. CO emissions follow Heald *et al.* [2004]. Background afternoon surface  $O_3$  is 10 to 20 ppb over Indonesia and relatively constant throughout the year. Ozone exceeds

50 ppb over India and downwind of Indochina in March, in northern China in summer, and in southern China in fall. Liu *et al.* [2002] presented detailed comparisons of an earlier version of GEOS-Chem with ozonesonde observations over Hong Kong and Japan in different seasons, and found in general good agreement. They showed that Asian biomass burning makes a major contribution to  $O_3$  south of  $32^\circ N$  in spring and that  $O_3$  outflow to the Pacific is greatest in spring and fall. Our simulation shows similar outflow features.

[45] Figure 10 shows the change in modeled surface ozone concentrations resulting from application of the top-down reactive NMVOC emission estimates constrained by GOME observations (Table 1 and Figure 3). The effects are small in the tropics where ozone production is strongly  $NO_x$ -limited. Although reactive biomass burning NMVOC emission is increased by over a factor of 4, surface  $O_3$  over Indochina and India increases by only 2–5 ppb. In contrast, simulated surface  $O_3$  levels in China are greatly influenced by the reactive NMVOC emissions. Martin *et al.* [2004a] used GOME HCHO/ $NO_2$  column concentration ratios to examine regional  $O_3$ - $NO_x$ -VOC sensitivity. They showed that northern China is  $NO_x$ -saturated (i.e., VOC-sensitive) from October to the following spring. This sensitivity to enhanced VOC is reflected by the 5 to 20 ppb  $O_3$  increase over eastern China year-round. Even in June when ozone production tends to be  $NO_x$ -limited, the very large increase in NMVOC emissions from the agricultural burning in the

North China Plain drives 5–20 ppb increases in surface ozone.

## 7. Conclusions

[46] This study demonstrates a new way to interpret HCHO column observations from space when multiple emission source types overlap in space and time. We used 1996–2001 satellite observations of HCHO columns from the GOME instrument as top-down constraints on reactive NMVOC emissions from east and south Asia. These reactive species include isoprene, alkenes, xylenes, and HCHO itself, which have sufficiently short lifetimes and prompt HCHO yields to provide local HCHO column signals detectable by GOME. A 6-year record of GOME HCHO column data was produced by purging anomalous solar days, cloudy scenes, and latitude-dependent bias. Air mass factors (AMFs) were obtained from the GEOS-Chem chemical transport model. The uncertainty of the resulting HCHO columns is 25–30% with no systematic bias according to previous comparisons with aircraft observations [Martin *et al.*, 2004b; Millet *et al.*, 2006]. The uncertainty is larger (up to a factor of 3) for biomass burning scenes, reflecting the role of aerosols. Millet *et al.* [2006] have previously demonstrated that HCHO columns measured from space constrain estimates of North American isoprene emissions in summer to within 40% for individual scenes.

[47] We compared the observed HCHO to simulated HCHO columns from the GEOS-Chem chemical transport model using state-of-science, bottom-up emission inventories from Streets *et al.* [2003a] for anthropogenic and biomass burning emissions and Guenther *et al.* [2006] for biogenic emissions (MEGAN). In extratropical winter when biogenic and biomass burning emissions are absent, the model produces above-background anthropogenic HCHO signals in large urban areas of central and southern China, and these are also seen in the GOME data. Comparison of GOME and GEOS-Chem values over China in winter shows high correlation ( $r^2 = 0.58$ ) and a 25% model underestimate. Independent in situ measurements of NMVOC/CO concentration ratios in Chinese cities suggest that this underestimate reflects vehicular emissions, including possibly a large direct emission of HCHO.

[48] Outside of extratropical winter, seasonal variability of GOME HCHO columns for different Asian regions is largely driven by biogenic and biomass burning emissions. We used the GEOS-Chem model to calculate the sensitivity of regional HCHO to each reactive NMVOC source type. The distinctive geographical and seasonal signatures from these emissions were then fitted to the GOME observation patterns with a linear model to produce top-down emission estimates. Isoprene emissions from east and south Asia inferred from GOME are  $56 \pm 30 \text{ Tg yr}^{-1}$ , slightly larger than the  $52 \text{ Tg yr}^{-1}$  from MEGAN. We find, however, that MEGAN is too low by a factor 3 for Chinese mixed forests and croplands, and too high for the tropical vegetation.

[49] GOME observations imply remarkably large biomass burning emissions of reactive NMVOCs throughout east and south Asia, almost 5 times higher than the Streets *et al.* [2003a] inventory. The largest discrepancy is for the North China Plain (NCP) in June, where GOME observes each year HCHO columns exceeding  $2.5 \times 10^{16} \text{ molecule cm}^{-2}$ ,

more than 10 times higher than the Streets *et al.* [2003a] estimate. This is due to previously unrecognized, in-field burning of crop residue following the winter wheat harvest, a practice recently developed as the need for biofuels diminishes. The NMVOC emission factors from this agricultural burning may be unusually high because of the density and moisture content of the residue.

[50] Total reactive NMVOC emission for east and south Asia constrained by GOME is  $83 \pm 32 \text{ Tg yr}^{-1}$ , compared to  $66 \text{ Tg yr}^{-1}$  from the bottom-up inventories. This reactive NMVOC emission significantly impacts the regional photochemistry simulation. In general, enhanced reactive NMVOC emissions lead to increased surface ozone, although the effect is small over the tropics because of  $\text{NO}_x$ -limited conditions. In contrast, Chinese surface  $\text{O}_3$  levels are very sensitive to the enhanced reactive NMVOC emissions. From late fall to spring, photochemistry in northern China is  $\text{NO}_x$ -saturated; surface  $\text{O}_3$  increases by as much as 20 ppb, despite the radiation being much weaker there than in the tropics in that time period. Although photochemistry in this region tends to be  $\text{NO}_x$ -limited between May and September [Martin *et al.*, 2004a], large  $\text{HO}_x$  production via HCHO from the reactive NMVOC species still drives 5–20 ppb surface  $\text{O}_3$  increases.

[51] **Acknowledgment.** This work was supported by the NASA Atmospheric Composition Modeling and Analysis Program.

## References

- Abbot, D. S., P. I. Palmer, R. V. Martin, K. V. Chance, D. J. Jacob, and A. Guenther (2003), Seasonal and interannual variability of North American isoprene emissions as determined by formaldehyde column measurements from space, *Geophys. Res. Lett.*, *30*(17), 1886, doi:10.1029/2003GL017336.
- Andreae, M. O., and P. Merlet (2001), Emission of trace gases and aerosols from biomass burning, *Global Biogeochem. Cycles*, *15*(4), 955–966.
- Arellano, A. F., Jr., P. S. Kasibhatla, L. Giglio, G. R. van der Werf, and J. T. Randerson (2004), Top-down estimates of global CO sources using MOPITT measurements, *Geophys. Res. Lett.*, *31*, L01104, doi:10.1029/2003GL018609.
- Barletta, B., S. Meinardi, F. S. Rowland, C. Chan, X. Wang, S. Zou, L. Y. Chan, and D. R. Blake (2005), Volatile organic compounds in 43 Chinese cities, *Atmos. Environ.*, *39*(32), 5979–5990.
- Bey, I., D. J. Jacob, R. M. Yantosca, J. A. Logan, B. Field, A. M. Fiore, Q. Li, H. Liu, L. J. Mickley, and M. Schultz (2001), Global modeling of tropospheric chemistry with assimilated meteorology: Model description and evaluation, *J. Geophys. Res.*, *106*, 23,073–23,096.
- Bloss, C., V. Wagner, A. Bonzanini, M. E. Jenkin, K. Wirtz, M. Martin-Reviejo, and M. J. Pilling (2005a), Evaluation of detailed aromatic mechanisms (MCMv3 and MCMv3.1) against environmental chamber data, *Atmos. Chem. Phys.*, *5*, 623–639.
- Bloss, C., et al. (2005b), Development of detailed chemical mechanism (MCMv3.1) for the atmospheric oxidation of aromatic hydrocarbons, *Atmos. Chem. Phys.*, *5*, 641–664.
- Burrows, J. P., et al. (1999), The Global Ozone Monitoring Experiment (GOME): Mission concept and first scientific results, *J. Atmos. Sci.*, *56*(2), 151–175.
- Cao, G., X. Zhang, D. Wang, and F. Zheng (2005a), Inventory of atmospheric pollutants discharged from biomass burning in China continent (in Chinese), *China Environ. Sci.*, *25*(4), 389–393.
- Cao, G., X. Zhang, D. Wang, and F. Zheng (2005b), Inventory of emissions of pollutants from open burning crop residue (in Chinese), *J. Agro Environ. Sci.*, *24*(4), 800–804.
- Carmichael, G. R., et al. (2003), Evaluating regional emission estimates using the TRACE-P observations, *J. Geophys. Res.*, *108*(D21), 8810, doi:10.1029/2002JD003116.
- Chameides, W. L., et al. (1999), Case study of the effects of atmospheric aerosols and regional haze on agriculture: An opportunity to enhance crop yields in China through emission controls?, *Proc. Natl. Acad. Sci. U. S. A.*, *96*(24), 13,626–13,633, doi:10.1073/pnas.96.24.13626.
- Chance, K., P. I. Palmer, R. J. D. Spurr, R. V. Martin, T. P. Kurosu, and D. J. Jacob (2000), Satellite observations of formaldehyde over North America from GOME, *Geophys. Res. Lett.*, *27*(21), 3461–3464.

- Christian, T. J., B. Kleiss, R. J. Yokelson, R. Holzinger, P. J. Crutzen, W. M. Hao, B. H. Saharjo, and D. E. Ward (2003), Comprehensive laboratory measurements of biomass-burning emissions: 1. Emissions from Indonesian, African, and other fuels, *J. Geophys. Res.*, *108*(D23), 4719, doi:10.1029/2003JD003704.
- Duan, F., Y. Lu, Y. Di, X. Liu, H. Zhang, X. Yang, and T. Yu (2001), Influence of straw burning on the air quality in Beijing (in Chinese), *Environ. Monit. China*, *17*(3), 8–11.
- Duncan, B. N., R. V. Martin, A. C. Staudt, R. Yevich, and J. A. Logan (2003), Interannual and seasonal variability of biomass burning emissions constrained by satellite observations, *J. Geophys. Res.*, *108*(D2), 4100, doi:10.1029/2002JD002378.
- European Space Agency, (1995), *The GOME User Manual*, ESA Publ. Div., Eur. Space Res. and Technol. Cent., Noordwijk, Netherlands.
- Goldstein, A. H., S. M. Fan, M. L. Goulden, J. W. Munger, and S. C. Wofsy (1996), Emissions of ethene, propene, and 1-butene by a midlatitude forest, *J. Geophys. Res.*, *101*(D4), 9149–9157.
- Guenther, A., et al. (1995), A global model of natural volatile organic compound emissions, *J. Geophys. Res.*, *100*(D5), 8873–8892.
- Guenther, A., T. Karl, P. Harley, C. Wiedinmyer, P. I. Palmer, and C. Geron (2006), Estimates of global terrestrial isoprene emissions using MEGAN (Model of Emissions of Gases and Aerosols from Nature), *Atmos. Chem. Phys.*, *6*, 3181–3210.
- Guo, H., T. Wang, D. R. Blake, I. J. Simpson, Y. H. Kwok, and Y. S. Li (2006), Regional and local contributions to ambient non-methane volatile organic compounds at polluted rural/coastal site in Pearl River Delta, China, *Atmos. Environ.*, *40*, 2345–2359, doi:10.1016/j.atmosenv.2005.12.011.
- Hao, W. M., and M. Liu (1994), Spatial and temporal distribution of tropical biomass burning, *Global Biogeochem. Cycles*, *8*, 495–503.
- Heald, C. L., D. J. Jacob, P. I. Palmer, M. J. Evans, G. W. Sachse, H. B. Singh, and D. R. Blake (2003), Biomass burning emission inventory with daily resolution: Application to aircraft observations of Asian outflow, *J. Geophys. Res.*, *108*(D21), 8811, doi:10.1029/2002JD003082.
- Heald, C. L., D. J. Jacob, D. B. A. Jones, P. I. Palmer, J. A. Logan, D. G. Streets, G. W. Sachse, J. C. Gille, R. N. Hoffman, and T. Nehrkorn (2004), Comparative inverse analysis of satellite (MOPITT) and aircraft (TRACE-P) observations to estimate Asian sources of carbon monoxide, *J. Geophys. Res.*, *109*, D23306, doi:10.1029/2004JD005185.
- Hirsch, R. M., and E. J. Gilroy (1984), Methods of fitting a straight line to data: Examples in water resources, *Water Res. Bull.*, *20*, 705–711.
- Horowitz, L. W., J. Liang, G. M. Gardner, and D. J. Jacob (1998), Export of reactive nitrogen from North America during summertime, *J. Geophys. Res.*, *103*(D11), 13,451–13,476.
- Houweling, S., F. Dentener, and J. Lelieveld (1998), The impact of non-methane hydrocarbon compounds on tropospheric photochemistry, *J. Geophys. Res.*, *103*(D9), 10,673–10,696.
- Jacob, D. J., B. D. Field, E. M. Jin, I. Bey, Q. Li, J. A. Logan, R. M. Yantosca, and H. B. Singh (2002), Atmospheric budget of acetone, *J. Geophys. Res.*, *107*(D10), 4100, doi:10.1029/2001JD000694.
- Jacob, D. J., B. D. Field, Q. Li, D. R. Blake, J. de Gouw, C. Warneke, A. Hansel, A. Wisthaler, H. B. Singh, and A. Guenther (2005), Global budget of methanol: Constraints from atmospheric observations, *J. Geophys. Res.*, *110*, D08303, doi:10.1029/2004JD005172.
- Jaeglé, L., R. V. Martin, K. Chance, L. Steinberger, T. P. Kurosu, D. J. Jacob, A. I. Modi, V. Yoboue', L. Sigha-Nkamdjou, and C. Galy-Lacaux (2004), Satellite mapping of rain-induced nitric oxide emissions from soils, *J. Geophys. Res.*, *109*, D21310, doi:10.1029/2004JD004787.
- Jaeglé, L., L. Steinberger, R. V. Martin, and K. Chance (2005), Global partitioning of NO<sub>x</sub> sources using satellite observations: Relative roles of fossil fuel combustion, biomass burning and soil emissions, *Faraday Disc.*, *130*, 407–423.
- Kanakidou, M., et al. (2005), Organic aerosol and global climate modelling: A review, *Atmos. Chem. Phys.*, *5*(4), 1053–1123.
- Klimont, Z., D. G. Streets, S. Gupta, J. Cofala, L. Fu, and Y. Ichikawa (2002), Anthropogenic emissions of non-methane volatile organic compounds in China, *Atmos. Environ.*, *36*(8), 1309–1322.
- Klinger, L. F., Q.-J. Li, A. B. Guenther, J. P. Greenberg, B. Baker, and J.-H. Bai (2002), Assessment of volatile organic compound emissions from ecosystems of China, *J. Geophys. Res.*, *107*(D21), 4603, doi:10.1029/2001JD001076.
- Koelemeijer, R. B. A., J. F. de Haan, and P. Stammes (2003), A database of spectral surface reflectivity in the range 335–772 nm derived from 5.5 years of GOME observations, *J. Geophys. Res.*, *108*(D2), 4070, doi:10.1029/2002JD002429.
- Kolb, C. E., S. C. Herndon, J. B. McManus, J. H. Shorter, M. S. Zahniser, D. D. Nelson, J. T. Jayne, M. R. Canagaratna, and D. R. Worsnop (2004), Mobile laboratory with rapid response instruments for real-time measurements of urban and regional trace gas and particulate distributions and emission source characteristics, *Environ. Sci. Technol.*, *38*, 5694–5703, doi:10.1021/es030718p.
- Korontzi, S., D. E. Ward, R. A. Susott, R. J. Yokelson, C. O. Justice, P. V. Hobbs, E. A. H. Smithwick, and W. M. Hao (2003), Seasonal variation and ecosystem dependence of emission factors for selected trace gases and PM<sub>2.5</sub> for southern African savanna fires, *J. Geophys. Res.*, *108*(D24), 4758, doi:10.1029/2003JD003730.
- Kurata, G., G. R. Carmichael, D. G. Streets, T. Kitada, Y. Tang, J.-H. Woo, and N. Thongboonchoo (2004), Relationships between emission sources and air mass characteristics in east Asia during the TRACE-P period, *Atmos. Environ.*, *38*(40), 977–997.
- Kurosu, T. P., K. V. Chance, and R. J. D. Spurr (1999), CRAG: Cloud Retrieval Algorithm for the European Space Agency's Global Ozone Monitoring Experiment, *Proceedings of the European Symposium of Atmospheric Measurements From Space*, pp. 513–521, Eur. Space Agency, Paris.
- Lee, C., Y. J. Kim, S. Hong, H. Lee, J. Jung, Y. Choi, J. Park, K. Kim, J. Lee, K. Chun, and H. Kim (2005), Measurement of atmospheric formaldehyde and monoaromatic hydrocarbons using differential optical absorption spectroscopy during winter and summer intensive periods in Seoul, Korea, *Water Air Soil Pollut.*, *166*, 181–195.
- Liu, H., D. J. Jacob, L. Y. Chan, S. J. Oltmans, I. Bey, R. M. Yantosca, J. M. Harris, B. N. Duncan, and R. V. Martin (2002), Sources of tropospheric ozone along the Asian Pacific Rim: An analysis of ozonesonde observations, *J. Geophys. Res.*, *107*(D21), 4573, doi:10.1029/2001JD002005.
- Liu, X., et al. (2006), First directly retrieved global distribution of tropospheric column ozone from GOME: Comparison with the GEOS-CHEM model, *J. Geophys. Res.*, *111*, D02308, doi:10.1029/2005JD006564.
- Martin, R. V., et al. (2002), An improved retrieval of tropospheric nitrogen dioxide from GOME, *J. Geophys. Res.*, *107*(D20), 4437, doi:10.1029/2001JD001027.
- Martin, R. V., D. J. Jacob, K. Chance, T. P. Kurosu, P. I. Palmer, and M. J. Evans (2003), Global inventory of nitrogen oxide emissions constrained by space-based observations of NO<sub>2</sub> columns, *J. Geophys. Res.*, *108*(D17), 4537, doi:10.1029/2003JD003453.
- Martin, R. V., A. M. Fiore, and A. Van Donkelaar (2004a), Space-based diagnosis of surface ozone sensitivity to anthropogenic emissions, *Geophys. Res. Lett.*, *31*, L06120, doi:10.1029/2004GL019416.
- Martin, R. V., D. D. Parrish, T. B. Ryerson, D. K. Nicks Jr., K. Chance, T. P. Kurosu, D. J. Jacob, E. D. Sturges, A. Fried, and B. P. Wert (2004b), Evaluation of GOME satellite measurements of tropospheric NO<sub>2</sub> and HCHO using regional data from aircraft campaigns in the southeastern United States, *J. Geophys. Res.*, *109*, D24307, doi:10.1029/2004JD004869.
- Martin, R. V., C. E. Sioris, K. Chance, T. B. Ryerson, T. H. Bertram, P. J. Wooldridge, R. C. Cohen, J. A. Neuman, A. Swanson, and F. M. Flocke (2006), Evaluation of space-based constraints on global nitrogen oxide emissions with regional aircraft measurements over and downwind of eastern North America, *J. Geophys. Res.*, *111*, D15308, doi:10.1029/2005JD006680.
- Meyer-Arneck, J., A. Ladstaetter-Weissenmayer, A. Richter, F. Wittrock, and J. P. Burrows (2005), A study of the trace gas columns of O<sub>3</sub>, NO<sub>2</sub> and HCHO over Africa in September 1997, *Faraday Disc.*, *130*, 387–405.
- Millet, D. B., et al. (2006), Formaldehyde distribution over North America: Implications for satellite retrievals of formaldehyde columns and isoprene emission, *J. Geophys. Res.*, *111*, D24S02, doi:10.1029/2005JD006853.
- Ministry of Agriculture of China (2007), Agricultural information database (in Chinese), Beijing. (Available at <http://zzys.agri.gov.cn/nongshi.asp>)
- Müller, J.-F., and G. Brasseur (1999), Sources of upper tropospheric HO<sub>2</sub>: A three-dimensional study, *J. Geophys. Res.*, *104*(D1), 1705–1715.
- Myneni, R. B., R. R. Nemani, and S. W. Running (1997), Estimation of global leaf area index and absorbed PAR using radiative transfer models, *IEEE Trans. Geosci. Remote Sens.*, *35*, 1380–1393.
- National Bureau of Statistics (2000), *China Statistical Yearbook 2000*, vol. 19, China Stat. Press, Beijing.
- Palmer, P. I., D. J. Jacob, K. Chance, R. V. Martin, R. J. D. Spurr, T. P. Kurosu, I. Bey, R. Yantosca, A. Fiore, and Q. Li (2001), Air-mass factor formulation for spectroscopic measurements from satellites: Application to formaldehyde retrievals from the Global Ozone Monitoring Experiment, *J. Geophys. Res.*, *106*, 14,539–14,550.
- Palmer, P. I., D. J. Jacob, A. M. Fiore, R. V. Martin, K. Chance, and T. P. Kurosu (2003a), Mapping isoprene emissions over North America using formaldehyde column observations from space, *J. Geophys. Res.*, *108*(D6), 4180, doi:10.1029/2002JD002153.
- Palmer, P. I., D. J. Jacob, D. B. A. Jones, C. L. Heald, R. M. Yantosca, J. A. Logan, G. W. Sachse, and D. G. Streets (2003b), Inverting for emissions of carbon monoxide from Asia using aircraft observations over the western Pacific, *J. Geophys. Res.*, *108*(D21), 8828, doi:10.1029/2003JD003397.
- Palmer, P. I., et al. (2006), Quantifying the seasonal and interannual variability of North American isoprene emissions using satellite observa-

- tions of the formaldehyde column, *J. Geophys. Res.*, *111*, D12315, doi:10.1029/2005JD006689.
- Park, R. J., D. J. Jacob, B. D. Field, R. M. Yantosca, and M. Chin (2004), Natural and transboundary pollution influences on sulfate-nitrate-ammonium aerosols in the United States: Implications for policy, *J. Geophys. Res.*, *109*, D15204, doi:10.1029/2003JD004473.
- Park, R. J., et al. (2005), Export efficiency of black carbon aerosol in continental outflow: Global implications, *J. Geophys. Res.*, *110*, D11205, doi:10.1029/2004JD005432.
- Poisson, N., M. Kanakidou, and P. J. Crutzen (2000), Impact of non-methane hydrocarbons on tropospheric chemistry and the oxidizing power of the global troposphere: 3-dimensional modelling results, *J. Atmos. Chem.*, *36*, 157–230.
- Richter, A., and T. Wagner (2001), Diffuser plate spectral structures and their influence on GOME slant columns, technical note, Inst. Environ. Phys., Univ. Bremen, Bremen, Germany.
- Richter, A., F. Wittrock, A. Ladstatter-Weissenmayer, and J. P. Burrows (2002), GOME measurements of stratospheric and tropospheric BrO, *Adv. Space Res.*, *29*(11), 1667–1672.
- Saunders, S. M., M. E. Jenkin, R. G. Derwen, and M. J. Pilling (2003), Protocol for the development of the Master Chemical Mechanism, MCM v3 (Part A): Tropospheric degradation of non-aromatic volatile organic compounds, *Atmos. Chem. Phys.*, *3*, 161–180.
- Sauvage, B., R. V. Martin, A. van Donkelaar, X. Liu, K. Chance, L. Jaeglé, P. I. Palmer, S. Wu, and T.-M. Fu (2007), Remote sensed and in situ constraints on processes affecting tropical tropospheric ozone, *Atmos. Chem. Phys.*, *7*, 815–838.
- Shim, C., Y. Wang, Y. Choi, P. I. Palmer, D. S. Abbot, and K. Chance (2005), Constraining global isoprene emissions with Global Ozone Monitoring Experiment (GOME) formaldehyde column measurements, *J. Geophys. Res.*, *110*, D24301, doi:10.1029/2004JD005629.
- Spurr, R. J. D., T. P. Kurosu, and K. V. Chance (2001), A linearized discrete ordinate radiative transfer model for atmospheric remote sensing retrieval, *J. Quant. Spectrosc. Radiat. Transfer*, *68*, 689–735.
- Steiner, A., C. Luo, Y. Huang, and W. L. Chameides (2002), Past and present-day biogenic volatile organic compound emissions in east Asia, *Atmos. Environ.*, *36*, 4895–4905.
- Strahler, A., D. Muchoney, J. Borak, M. Friedl, S. Gopal, E. Lambin, and A. Moody (1999), MODIS land cover product algorithm theoretical basis document (ATBD), version 5.0, MODIS land cover and land-cover change, 72 pp., Boston Univ., Boston, Mass.
- Streets, D. G., et al. (2003a), An inventory of gaseous and primary aerosol emissions in Asia in the year 2000, *J. Geophys. Res.*, *108*(D21), 8809, doi:10.1029/2002JD003093.
- Streets, D. G., K. F. Yarber, J.-H. Woo, and G. R. Carmichael (2003b), Biomass burning in Asia: Annual and seasonal estimates and atmospheric emissions, *Global Biogeochem. Cycles*, *17*(4), 1099, doi:10.1029/2003GB002040.
- Suntharalingam, P., D. J. Jacob, P. I. Palmer, J. A. Logan, R. M. Yantosca, Y. Xiao, M. J. Evans, D. G. Streets, S. L. Vay, and G. W. Sachse (2004), Improved quantification of Chinese carbon fluxes using CO<sub>2</sub>/CO correlations in Asian outflow, *J. Geophys. Res.*, *109*, D18S18, doi:10.1029/2003JD004362.
- Turquet, S., et al. (2007), Inventory of boreal fire emissions for North America in 2004: Importance of peat burning and pyroconvective injection, *J. Geophys. Res.*, doi:10.1029/2006JD007281, in press.
- Van Aardenne, J. A., F. J. Dentener, J. G. J. Olivier, J. A. H. W. Peters, and L. N. Ganzeveld (2005), The EDGAR 3.2 Fast Track 2000 dataset (32FT2000). (Available at [http://www.rivm.nl/edgar/Images/Description\\_of\\_EDGAR\\_32FT2000\(v8\)\\_tcm32-22222.pdf](http://www.rivm.nl/edgar/Images/Description_of_EDGAR_32FT2000(v8)_tcm32-22222.pdf))
- Wang, T., et al. (2004), Relationships of trace gases and aerosols and the emission characteristics at Lin'an, a rural site in eastern China during spring 2001, *J. Geophys. Res.*, *109*, D19S05, doi:10.1029/2003JD004119.
- Wang, Y. X., M. B. McElroy, T. Wang, and P. I. Palmer (2004), Asian emissions of CO and NO<sub>x</sub>: Constraints from aircraft and Chinese station data, *J. Geophys. Res.*, *109*, D24304, doi:10.1029/2004JD005250.
- Wiedinmyer, C., A. Guenther, P. Harley, N. Hewitt, C. Geron, P. Artaxo, R. Steinbrecher, and R. Rasmussen (2004), Global organic emissions from vegetation, in *Emissions of Atmospheric Trace Compounds*, edited by C. Granier, P. Artaxo, and C. Reeves, pp. 115–170, Springer, New York.
- Xiao, Y., D. J. Jacob, J. S. Wang, J. A. Logan, P. I. Palmer, P. Suntharalingam, R. M. Yantosca, G. W. Sachse, D. R. Blake, and D. G. Streets (2004), Constraints on Asian and European sources of methane from CH<sub>4</sub>-C<sub>2</sub>H<sub>6</sub>-CO correlations in Asian outflow, *J. Geophys. Res.*, *109*, D15S16, doi:10.1029/2003JD004475.

B. Barletta and D. R. Blake, Department of Chemistry, University of California, Irvine, CA 92697-2025, USA.

K. Chance, Harvard-Smithsonian Center for Astrophysics, Cambridge, MA 02138, USA.

T.-M. Fu, D. J. Jacob, and Y. X. Wang, Department of Earth and Planetary Sciences, Harvard University, Cambridge, MA 02138, USA. (fu@fas.harvard.edu)

P. I. Palmer, School of GeoSciences, University of Edinburgh, Edinburgh EH9 3JW, UK.

M. J. Pilling and J. C. Stanton, Department of Chemistry, University of Leeds, Leeds LS2 9JT, UK.